PROCEEDINGS OF ECOS 2023 - THE 36TH INTERNATIONAL CONFERENCE ON
EFFICIENCY, **C**OST, **O**PTIMIZATION, **S**IMULATION AND ENVIRONMENTAL IMPACT OF ENERGY SYSTEMS
25-30 JUNE 2023, LAS PALMAS DE GRAN CANARIA, SPAIN

Modelling and Scaling Laws of cryogenic tank's thermal response to sloshing

Samuel Ahizi[a], Pedro A. Marques[b,c], Miguel A. Mendez[b]

[a] von Karman Institute, Waterloosesteenweg 72, 1640 Sint-Genesius-Rode, Belgium, samuel.ahizi@vki.ac.be, CA
[b] von Karman Institute, Waterloosesteenweg 72, 1640 Sint-Genesius-Rode, Belgium
[c] Université Libre de Bruxelles, Av. Franklin Roosevelt 50, 1050 Bruxelles, Belgium

Abstract:

The storage of cryogenic fuels such as liquid hydrogen (LH_2) or liquefied natural gas (LNG) poses significant thermal and mechanical loads to the tanks that store them because of the considerable temperature gradients produced during filling operation and sloshing. This work presents a numerical investigation of the transient heat conduction within the walls of an insulated cryogenic tank undergoing sloshing. The unsteady heat conduction is analyzed by modeling the sloshing as a spatially distributed and time-varying boundary condition on the inner side of the tank. The scaling laws of the problem are analyzed by combining the characteristic time scale of heat conduction with the characteristic time scales of the sloshing. The modulation of sloshing-induced thermal fluctuations is then analyzed across the wall thickness and in the circumferential direction. The resulting dimensionless modulation map allows for analyzing the tank's thermal response for different designs.

Keywords:

Cryogenics, Cryogenic liquid storage, Heat transfer and thermal insulation, Sloshing,

1. Introduction

Cryogenic tanks store liquefied fuels such as liquid hydrogen (LH_2) or liquefied natural gas (LNG) at extremely low temperatures, ranging from 20 to 110 K. Consequently, the walls of these tanks experience significant temperature gradients during all the phases of their operating cycle (e.g., chill-down, filling, pressurization), and the design and optimization of their thermal response raise many challenges. The tank wall and the insulation layers should minimize the heat ingress to minimize the boil-off of the cryogenic liquid and, thus, the need for venting to avoid overpressurizing the tank. Moreover, the tank weight should be minimized in all transport applications to maximize the payload without compromising its mechanical resistance. The need for these compromises has motivated various experimental and numerical investigations on the thermo-mechanical analysis of these tanks.

Heathman et al. [1] experimentally characterized a cryogenic tank for space applications and measured the effect of boil-off and different insulation strategies on the wall temperature. Murugan, Starvin, and Dhas[2], the authors studied the behavior of a hydrogen tank during the chill-down process using thermo-structural finite elements analysis to estimate the heat transfer and induced deformations. Similarly, Rao and Jagadeesh [3], and Ko [4] used finite elements to characterize the structural and thermal stress of a hydrogen tank under high-pressure loads and heating/cryogenic cooling. Craig and Hanna [5] studied the thermal response of a LH_2 tank subjected to extreme heating profiles using 1D/2D finite differences models to determine the boil-off level as a function of the insulation strategy.

Furthermore, the inner tank material in contact with the fluid must be carefully chosen, especially for hydrogen storage, as its molecules are likely to penetrate through the solid [6] and embrittle the materials [7, 8]. This has promoted using metallic materials such as stainless steel, aluminum alloys, and nickel alloys, combined with multilayer and vacuum insulation [9]. The latter consists of alternating layers of reflective and insulating materials to minimize radiation and conduction heat transfer. For hydrogen tanks, an aluminum alloy inner layer offers a slow permeation rate and is less subject to embrittlement [10]. Such an approach was also shown to minimize boil-off due to "hot spots" by spreading the localized heat leaks through the metal's high conductivity [11]. In the aforementioned studies, the effect of sloshing has not been considered by focusing either on static storage or a perfectly mixed tank. However, an appreciable temperature difference (up to 15 K, [12, 13]) can be produced between the liquid and the ullage gas. Sloshing can thus induce additional time-varying thermal loads on the tank's wall [14]. This is especially critical in metallic alloys, which are known to suffer from crack propagation and *thermal fatigue* when undergoing repeated thermal cycles [15].

https://doi.org/10.52202/069564-0032

This work investigates the thermal response of a horizontal cylindrical tank undergoing lateral sloshing. We consider a simplified model in 2D, leveraging the large aspect ratios in most common tank designs and allowing for fast numerical integration of the heat conduction problem. The thermal response is analyzed in a dimensionless form to link the modulation of temperature fluctuations to the dimensionless numbers scaling the problem.

The rest of the article is structured as follows. Section 2. introduces the problem set, with its simplifying assumptions and the numerical methods and investigated test cases. Section 3. collects the results regarding thermal propagation across the wall's thickness and along the circumferential direction. Finally, section 4. collects conclusions and perspectives for future work.

2. Problem set

The configuration investigated in this work is illustrated in the schematic of Fig. 1a. We consider a horizontal cylindrical tank with radius R and thickness e_1, insulated with a cylindrical shell of thickness e_2 and filled with a liquid up to a level f. The extension of the tank along its axis (i.e. orthogonal to the paper) is large enough to allow considering the problem in 2D, in the plane (x, y) introduced in the figure.

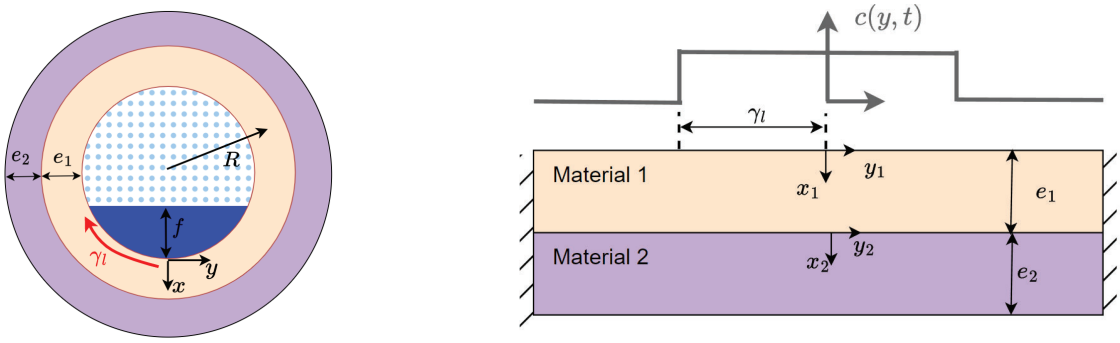

(a) Cross view of the cylinder

(b) Two-dimensional simplification of the tank wall geometry

Figure 1: Schematic views of the tank geometry and 2D domain considered in this work.

Assuming that the tank's thickness is much smaller than its circumference (i.e. $e_1, e_2 \ll 2\pi R$), we replace the curvilinear coordinates with Cartesian ones and construct a 2D domain by unwrapping the cylinder and the shell (see Fig. 1b). We treat the heat conduction problem in the cylinder and the insulation shell with two distinct domains, herein distinguished with subscripts 1 and 2.

On the inner side of the wall, in contact with the liquid and ullage gas, we define the fluid temperature as $T_f(y_1, t) = T_l c(y_1, t) + T_g(1 - c(y_1, t))$, where T_l and T_g are the (constant) temperatures on the liquid and the ullage gas respectively and $c(y_1, t) \in [0, 1]$ is a color function equal to 1 where the solid is contact with the liquid and 0 when it is contact with the gas. The temperature difference $\Delta T = T_g - T_l$ is encountered in cryogenic tanks because of heat leaks and/or pressurization as well as evaporation and the natural tendency of the liquid to be subcooled with respect to the interface [12, 13]. By keeping the temperature of the fluids constant in time, we assume no thermal mixing and no mass exchange (evaporation/condensation) between the two phases, at least within the sloshing time scale of interest.

The 2D heat conduction problem and the boundary conditions considered in this work for the two domains $\Omega_1 := x_1 \in [0, e_1] \times y_1 \in [-\pi R, \pi R]$ and $\Omega_2 := x_2 \in [0, e_2] \times y_2 \in [-\pi R, \pi R]$ are

$$
\begin{cases}
\partial_t T_1(x_1, y_1, t) & = \alpha_1(\partial^2_{x_1} T_1 + \partial^2_{y_1} T_1) \\
T_1(0, y_1, t) & = T_f(y_1, t) \\
\quad \text{or} & \\
\kappa_1 \partial_x T_1(0, y_1, t) & = h_f(T_1(0, y_1, t) - T_f(y_1, t)) \\
T_1(e_1, y_1, t) & = T_2(0, y_2, t) \\
T_1(x_1, -\pi R, t) & = T_1(x_1, \pi R, t)
\end{cases}
\quad \text{and} \quad
\begin{cases}
\partial_t T_2(x_2, y_2, t) & = \alpha_2(\partial^2_{x_2} T_2 + \partial^2_{y_2} T_2) \\
T_2(0, y_2, t) & = T_1(e_1, y_1, t) \\
\kappa_2 \partial_x T_2(e_2, y_2, t) & = h_a(T_2(e_2, y_2, t) - T_a) \\
T_2(x_2, -\pi R, t) & = T_2(x_2, \pi R, t)
\end{cases}
\tag{1}
$$

https://doi.org/10.52202/069564-0032

where α_1, α_2 are the heat diffusivities, and κ_1, κ_2 are the thermal conductivities for the two materials. On the inner condition problem, we consider two scenarios for the boundary conditions on the surface in contact with the fluid: (1) a Dirichlet boundary condition or (2) a Robin boundary condition with heat transfer coefficient h_f. The assumption of Dirichlet conditions on the inner wall is purely demonstrative and rather unphysical. Considering the large differences in the thermal effusivities of the fluid (whether liquid or gas) and the solid, the surface temperature at the contact between the two is expected to be much closer to the latter than the former. However, from the thermal loading point of view, the two investigated problems can be seen as the two extremes between the actual loads are expected.

The two solid domains communicate with a Dirichlet boundary condition at $x_1 = e_1$, $x_2 = 0$ while a Robin boundary condition is considered on the external surface of the insulation, with heat transfer coefficient h_a. Periodic boundary conditions are introduced in $y = -\pi R$ and $y = \pi R$ for both domains, as both locations are at the top of the cylinder.

To model the occurrence of a sloshing event, we treat the color function with an imposed variation in space and time (see Fig. 1b). This is a square wave with half-width γ_l, oscillating with an amplitude A_f and an angular frequency ω. Focusing on lateral sloshing, the oscillation frequency is taken as the one corresponding to the first sloshing mode in potential flow theory [16]. This is usually the first to be triggered and most prominently present in the sloshing response. According to Lamb[17] for an horizontal tank this is $\omega = \sqrt{1.37g/(R - e_1)}$, with g the gravitational acceleration. Concerning the sloshing amplitude A_f and width γ_l, computed from the filling level. Throughout the modeling of the sloshing, we focus on planar waves [16]. Furthermore, the temperature of the fluids is kept constant, thus assuming no thermal mixing between the two phases. Finally, evaporation due to heat ingress or condensation due to thermal mixing are not considered.

2.1. Scaling and dimensionless formulation

To scale the problem, we consider the dimensionless coordinates $\hat{x}_j = x_j/e_j$ and $\hat{y}_j = y_j/2\pi R$, with $j = 1, 2$, the dimensionless temperatures $\theta_j = (T_j - T_l)/(T_g - T_l)$, and the dimensionless time $\hat{t} = \omega t/2\pi$. The resulting dimensionless problem in $\hat{\Omega}_1 := x_1 \in [0,1] \times \hat{y}_1 \in [-1/2, 1/2]$ and $\hat{\Omega}_2 := \hat{x}_2 \in [0,1] \times \hat{y}_2 \in [-1/2, 1/2]$ becomes:

$$\begin{cases} \partial_t \theta_1(\hat{x}_1, \hat{y}_1, \hat{t}) & = Fo_1(\partial^2_{\hat{x}_1}\theta_1 + \varepsilon_1^2 \partial^2_{\hat{y}_1}\theta_1) \\ \theta_1(0, \hat{y}_1, \hat{t}) & = 1 - c(\hat{y}_1, \hat{t}) \\ \quad \text{or} & \\ \partial_{\hat{x}_1}\theta_1(0, \hat{y}_1, t) & = Nu_f(\theta_1(0, \hat{y}_1, t) - 1 + c(\hat{y}_1, \hat{t})) \\ \theta_1(1, \hat{y}_1, \hat{t}) & = \theta_2(0, \hat{y}_2, \hat{t}) \\ \theta_1(\hat{x}_1, -1/2, \hat{t}) & = \theta_1(\hat{x}_1, 1/2, \hat{t}) \end{cases} \quad \text{and} \quad \begin{cases} \partial_t \theta_2(\hat{x}_2, \hat{y}_2, \hat{t}) & = Fo_2(\partial^2_{\hat{x}_2}\theta_2 + \varepsilon_2^2 \partial^2_{\hat{y}_2}\theta_2) \\ \theta_2(0, \hat{y}_2, \hat{t}) & = \theta_1(1, \hat{y}_1, \hat{t}) \\ \partial_{\hat{x}_2}\theta_2(1, \hat{y}_2, \hat{t}) & = Nu_a(\theta_2(1, \hat{y}_2, \hat{t}) - \theta_a) \\ \theta_2(\hat{x}_2, -1/2, \hat{t}) & = \theta_2(\hat{x}_2, 1/2, \hat{t}) \end{cases} \tag{2}$$

where $Fo_j = 2\pi\alpha_j/(e_j^2\omega)$ are the Fourier numbers in the two domains, $Nu_f = h_f e_1/\kappa_1$ and $Nu_a = h_a e_2/\kappa_2$ are the Nusselt numbers in the inner and outer surfaces, and $\varepsilon_j = e_j/2\pi R$ are the thickness to circumference ratio of the two domains.

The Nusselt number on the outer surface was computed using a classic correlation of natural convection over on horizontal cylinder [18]:

$$Nu_a = \left(0.6 + \frac{0.387 Ra_a^{1/6}}{[1 + (0.559/Pr_a)^{9/16}]^{8/27}}\right)^2 \tag{3}$$

where $Ra_a = g\beta_a(T_a - T_2(e_2)(D_o)^3)/(\nu_a^2)Pr_a$ is the Rayleigh number based on the outer diameter $D_o = 2R + e_1 + 2e_2$ as a reference length, the external wall temperature $T_2(e_2)$. This is computed during the simulation and the air properties at ambient temperature while the air's Prandtl number at ambient temperature Pr_a is constant.

The Nusselt number on the inner surface is computed using two correlations depending on the inner Richardson number :

$$Ri_f = \frac{Gr_f}{Re_r^2} = \frac{g\beta_f(T_a - T_1(0))(R_i)^3)}{A_f^4\omega^2} \tag{4}$$

where the Reynolds number was defined as in [19] and the properties β_f and ν_f and Pr_f are computed using the color function $c(y_1, t)$ for weight-averaging liquid and gas properties. Natural convection is considered $Ri > 10$, while forced convection is assumed if $Ri_f < 0.1$ [20]. A mixed regime appears between these two boundaries.

https://doi.org/10.52202/069564-0032

Therefore, depending on Ri_f the Nusselt number on the inner surface is

$$\begin{cases} Nu_f = Nu_{f,F} = 0.680 Re^{1/2} Pr^{1/3} & \text{if } Ri < 0.1 \\ Nu_f = Nu_{f,N} = 0.605 Ra_f^{1/3} & \text{if } Ri > 10 \\ Nu_f = (Nu_{f,F}^3 + Nu_{f,N}^3)^{1/3} & \text{if } Ri \in [0.1, 10] \end{cases} \tag{5}$$

All fluid properties used in the above correlations were computed from the library *CoolProp* [21] using air for the ambient side and liquid/gaseous hydrogen or methane for the fluid side. Typical values for the thermophysical properties of the materials considered in this work are summarized in Table 1 while the usual ranges for the Nusselt numbers are given in Table 2.

Table 1: Properties and typical thickness of the materials considered in the composition of the walls.

Material	κ [W/m/K]	α [mm^2/s]	e [mm]
Al 6061 (domain 1) [22]	162	65.4	1-20
SST 316 (domain 1) [22]	16.3	4.1	1-20
Polyurethane foam (domain 2) [23]	0.05	2.2	10-200
High Density Polyethylene (domain 2) [24]	0.04	0.02	10-200

Table 2: Typical Nusselt number range

Fluid	Gas phase	Liquid phase
Air	70-140	-
Hydrogen	100-2500	6000-10000
Oxygen	100-1200	6800 - 7300
Methane	100-800	3800 - 4300

2.2. Numerics and selected test cases

The problems in (2) were solved using the method of lines. This approach consists of discretizing the equation's spatial derivatives and transforming the resulting expressions into a system of ordinary differential equations (ODEs) in time. The spatial derivatives were computed using second-order finite difference while the time integration was carried out using the LSODA solver [25] from the ODEINT package in SciPy [26]. Prior to introducing the sloshing perturbation, the thermal field is initialized with the steady solution at rest, i.e., without fluid motion.

We consider two aspects of the tank's thermal response. First, we focus on the thermal response across the wall thickness. To this end, we reduce the problem to a 1D domain by setting $\varepsilon_1, \varepsilon_2 \to 0$ in (2) and study the dimensionless temperature evolution at the height of the interface at rest, that is $\hat{y}_1 = \gamma_l$). For the half-filled tanks considered in this work, this is $\hat{y}_1 = 1/4$ (or $\hat{y}_1 = -1/4$). In this location, the oscillation of the color function in the dimensionless domain $c(\gamma_l/(2\pi R), \hat{t})$ produces a square wave of unitary amplitude, unitary period and 50% duty cycle (see Fig. 2). Second, we focus on the circumferential propagation of heat by analyzing the full 2D problem. Considering a half-filled tank, the interface is centered at $\hat{y}_1 = \pm 1/4$ and oscillates harmonically in time with unitary period and dimensionless amplitude $\hat{A}_f$. An example of the corresponding spatiotemporal evolution for an amplitude $\hat{A}_f = 0.2$ is shown in Fig. 2.

Table 3: Test matrix summarizing the main parameters for the 1D and 2D simulations presented in this work.

Case	Model	θ_a	ε_1	ε_2	Fo_1	Fo_2	Fluid BC	No. layers
1	1D	28.8	0	0	[7e-5, 300]	-	Dirichlet	1
2	1D	28.8	0	0	[7e-5, 300]	-	Robin	1
3	1D	28.8	0	0	[1e-3, 80]	[1e-5, 30]	Robin	2
4	2D	28.8	1e-3	7e-3	5e-2	6	Robin	2

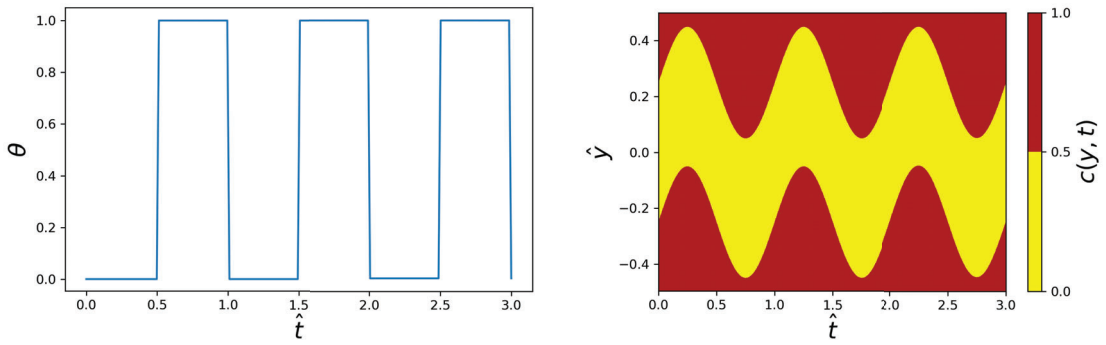

(a) (b)

Figure 2: (a) Dimensionless temperature evolution at $\hat{y}_1 = \gamma_l$ in the 1D problem and (b) spatiotemporal evolution of the color function used to simulate sloshing $c(y, t)$ in the 2D problem. In both cases, the tank is considered to be half-filled.

The simulations were carried out with $n_x = 100$ grid points across the thickness ($\hat{x}$) and $n_y = 70$ points across the circumferential coordinate ($\hat{y}$) for a total of 10 oscillation periods. A grid dependence study proved that this discretization was sufficient for our needs. Four test cases are considered, and their settings are reported in Table 3. Case 1 considers a 1D problem with a single layer, with Fourier numbers ranging from 7×10^{-5} to 300. To give an order of magnitude, a representative Al6061 tank from [27], with $R = 0.5$ m and $e_1 = 5$ mm (see Table 1), shielded by a shell of $e_2 = 3$ cm thick Polyurethan foam leads to $Fo_1 \approx 6$ and $Fo_2 \approx 5 \times 10^{-3}$. Dirichlet boundary conditions are considered in Case 1, with a dimensionless ambient temperature of $\theta_a = 28.8$. This represents a test case with $T_l = 20$K, $T_a = 293$K, and $\Delta T = T_g - T_l = 10$ K. Case 2 is identical to Case 1 but considers Robin boundary conditions in the inner wall. Case 3 considers a multi-layer problem, maintaining the 1D formulation, while Case 4 considers the multi-layer problem using a 2D formulation.

To quantify the dimensionless thermal response of the tank wall to the sloshing-induced thermal excitation, we define the dimensionless thermal modulation as

$$\mathcal{H}(\hat{x}, \hat{y}) = \max(\theta(\hat{x}, \hat{y})) - \min(\theta(\hat{x}, \hat{y})). \tag{6}$$

This is only a function of $\hat{x}$ in the 1D problem (having fixed $\hat{y} = \pm 1/4$). Moreover, we define the thermal penetration depth as the distance from $\hat{x}_1 = 0$, or $\hat{x}_2 = 0$, along the wall thickness, within which $\mathcal{H} > 0.1$, hence $\mathcal{H}(\hat{x} = \hat{d}) = 0.1$.

3. Results and discussion

The results for the one-dimensional simulations (Cases 1,2,3 in Table 1) are presented in section 3.1. while the results for the two-dimensional simulations (Cases 4 in Table 1) are presented in section 3.2..

3.1. One-dimensional model

3.1.1. Single layered tank wall response to sloshing excitation

Focusing on the single-layered wall (Cases 1 and 2 in Table 1), Fig. 3a and 3b show the distribution of $\mathcal{H}$ across the tank's thickness $\hat{x}$ with the Dirichlet and Robin boundary conditions on the inner wall, respectively, for a broad range of Fourier numbers. Since only one layer is considered, no subscripts are used in the legends. The colored area in both figures defines the region $\mathcal{H} < 0.1$, indicating where the sloshing-induced thermal oscillations are considered negligible.

These figures show that the penetration depth $\hat{d}$ remains identical with both boundary approaches. Furthermore, in both cases, for $Fo > 3 \times 10^{-1}$, the sloshing perturbation causes the thermal oscillations to propagate through the entire thickness, producing $\mathcal{H}(1) \sim 1$. Then, as $Fo \to 0$, the thermal fluctuations are increasingly damped, pushing the penetration depth to zero (i.e., $\hat{d} \to 0$). In such a case, the time scale of the sloshing excitation is negligible compared to the time scale of diffusion. In fact, as $Fo < 10^{-2}$, the perturbations are significantly damped in the close vicinity of the wall.

The key difference between Cases 1 and 2 is the value of the thermal modulation in the vicinity of the inner wall (i.e., $\mathcal{H}(0)$). While the Dirichlet condition imposes the perturbation to be bounded between 0 and 1, the convective boundary condition can amplify it beyond these bounds. This means that the inner wall becomes

https://doi.org/10.52202/069564-0032

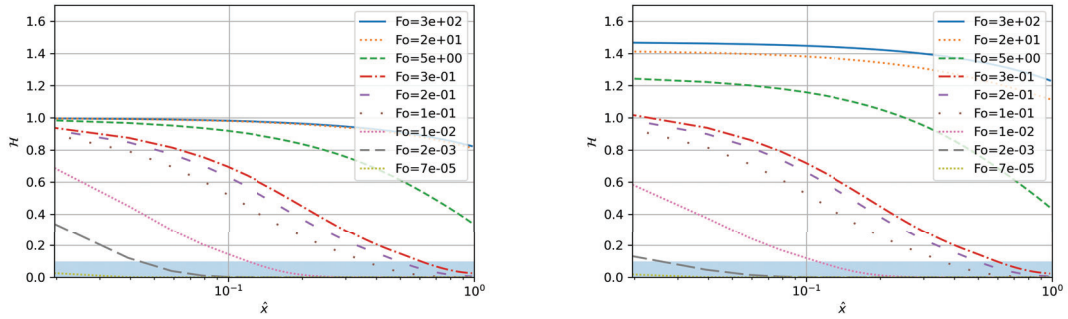

(a) (b)

Figure 3: One-dimensional transfer function along non-dimensional wall thickness for different *Fo* numbers. (a) Dirichlet boundary condition on the fluid side and (b) Robin boundary condition on the fluid side.

warmer than the gas. One can show that the steady state solution of the 1D heat equation (2) with Robin boundary conditions on both ends leads to the following inner wall temperature:

$$\overline{\theta}(0) = \frac{(Nu_f Nu_a - Nu_f)\,(1 - \overline{c}(\gamma_l)) + Nu_a \theta_a}{Nu_f Nu_a + Nu_a - Nu_f}. \tag{7}$$

Therefore, provided that $\theta_a > 1$, the inner temperature is always warmer than the fluid at equilibrium, i.e. $\overline{\theta}(0) > 1 - \overline{c}(\gamma_l)$ with $\overline{c}(\gamma_l) = 0$ for the gas and 1 for the liquid. From Equation (7), it is clear that temperature overshoot increases as Nu_f decreases. Thus, since the Nusselt number of the gas is one order of magnitude lower than the liquid's (see Table 2), the temperature overshoot in the regions in contact with the gas is larger than in the liquid phase. Consequently, as shown in Fig. 3b, the thermal modulation reaches values greater than unity for $Fo > 3 \times 10^{-1}$.

This phenomenon is more evident in Fig. 4, which shows the dimensionless evolution of temperature in time at $\hat{x}_1 = 0, 0.5, 1$ with Dirichlet (a) and Robin (b) boundary conditions for $Fo = 3.9$. This case is representative of an aluminum layer within the typical thickness in Table 1. The Robin boundary condition introduces a delay in the transfer of the perturbation to the inner side of the wall, as depicted by the solid line in Fig. 4b. This delay further attenuates the perturbation when the time scale of the excitation is much smaller than the one of diffusion, i.e. $Fo << 1$, compared to the Dirichlet approach. This effect can be visualized for $Fo = 10^{-2}$ and $Fo = 2 \times 10^{-3}$ on Fig. 3.

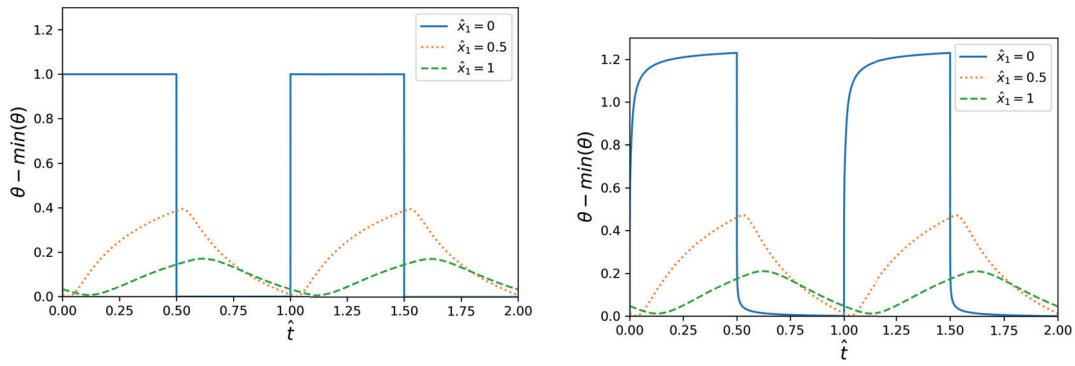

(a) (b)

Figure 4: Evolution of the temperature with dimensionless time at different depths of the single-layered wall, $Fo = 3.9$. (a) Dirichlet boundary condition on the fluid side and (b) Robin boundary condition on the fluid side.

While the Dirichlet simplification provides a good estimate of the penetration depth and allows for identifying the critical Fourier number above which the perturbation reaches the ambient side as $Fo = 3 \times 10^{-1}$, it fails

at representing the amplification/attenuation phenomena. Indeed, as this approach forces the inner side of the wall to be at the fluid temperature, the wall overheating due to external heat flux cannot be considered. In addition, the delay introduced by the thermal inertia is under-predicted. In the following, we focus on the convective boundary condition on the fluid side.

3.1.2. Multi-layered tank wall response to sloshing excitation

As cryogenic tanks are usually made of multi-layered materials, we investigate the influence of the different layer compositions and thicknesses for the dual-layered tank (Case 3 in Table 3). To represent the state-of-art tank layout, a conductive material is placed on the fluid side while an insulating material is placed on the ambient side. Thus, we study the thermal response of the two layers as a function of their respective Fourier numbers for the ranges indicated in Table 3. Figure 5 shows contour maps of the penetration depth within the two layers as a function of the Fourier number combination. Similarly, Fig. 7 represents the maximum value of thermal modulation encountered in each layer, i.e. $\mathcal{H}_1(0)$ and $\mathcal{H}_2(0)$. In these figures, the circle and cross points locate existing hydrogen tanks of respective dimensions $R \approx 0.5$ meters [27] and $R \approx 1.5m$ [28]. The dimensionless temperature evolution of the circle point is depicted in Fig. 6.

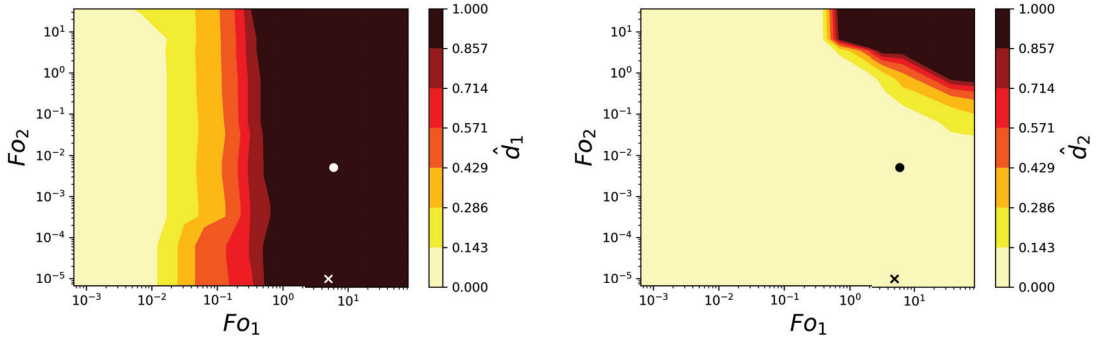

(a) (b)

Figure 5: Contour plot of dimensionless penetration depths of a dual-layered cryogenic tank wall as a function of the layer *Fo* numbers. (a) Penetration depth on the fluid side material and (b) penetration depth on the ambient side material

Figure 5a shows the penetration depth in the first layer (material 1 in Figure 1), computed as in the previous condition, while Figure 5b shows the same quantity in the second layer (material 2 in Figure 1). The thermal fluctuation reaches the second layer by traveling the first layer only if $Fo_1 > 3 \times 10^{-1}$. When this occurs, the fluctuation can travel through the second layer if $Fo_2 > 10^{-1}$ (note that one has $\hat{d}_2 > 1/3$ for $Fo_2 > 10^{-1}$ 5b).

Figures 6 shows the dimensionless temperature fluctuation at $\hat{x}_1 = 0, 0.5, 1$ for the multilayer condition in the case of $Fo_1 = 3.9$, $Fo_2 = 10^{-5}$ (configuration labelled with a circle in figures 5). In this condition, the oscillation period is large enough to let the wall reach equilibrium before the solid comes into contact with a different

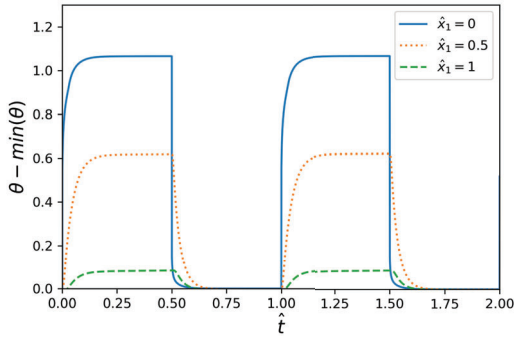

Figure 6: Evolution of the temperature with dimensionless time at different depths of the fluid side material for a dual-layered wall, $Fo_1 = 3.9$, $Fo_2 = 10^{-5}$ (circle marker in Figure 5).

https://doi.org/10.52202/069564-0032

phase. Figures 7a and 7b show the maximum value of the dimensionless modulation $\mathcal{H}$ in both materials for the same range of Fourier numbers considered in the previous figures. These figures show that the penetration length for the inner material is almost independent of the outer one, but the amplification in the inner (more conductive) material is influenced by the Fourier number of the outer (insulation) layer. The amplification of the thermal oscillation is reduced as $Fo_2 \to 0$. As Fo_2 tends to 0, the ambient side material mitigates the external heat ingress, thus tempering the overheating of the inner side with respect to the ullage gas. It is interesting to note that the insulation layer always receives an attenuated perturbation, as depicted in Fig. 7b, except for extreme Fourier number values, i.e. $Fo_{1,2} > 10$.

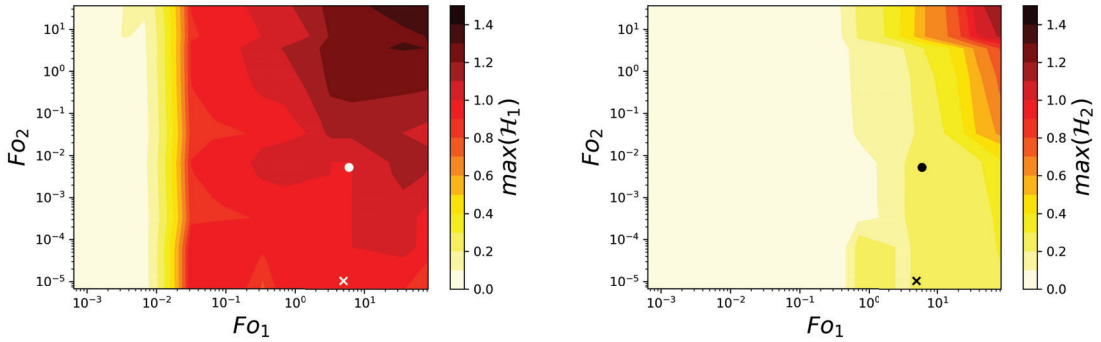

(a) (b)

Figure 7: Contour plot of dimensionless thermal modulation of a dual-layered cryogenic tank wall as a function of the layer *Fo* numbers, (a) maximum value in fluid side material, and (b) maximum value in the ambient side material

3.2. Two-dimensional model

We conclude this investigation with the two-dimensional response of the wall to sloshing with varying dimensionless excitation amplitudes $\hat{A}_f$. We focus on the configuration with $Fo_1 = 3.9$, $Fo_2 = 10^{-5}$ (circle marker in Fig. 5) because similar results were found for the one with $Fo_1 = 3.9$, $Fo_2 = 10^{-5}$ (cross marker in Fig. 5).

The resulting thermal modulation maps in 2D are depicted in Fig. 8a. The boundary between the two materials is represented by a horizontal solid line, while vertical dashed lines delimit the region spanned by the oscillation of the temperature distribution (color function). The results of the 2D approach align with the maps 7 and 5. Indeed, while the perturbation enters the insulation layer with a thermal modulation $\mathcal{H}_2 \approx 0.4$, it is quickly damped so that $\hat{d}_2 \approx 0$. Regardless of the oscillation amplitude, and despite the large diffusivity of the inner layer, we observe that the response of the wall remains extremely localized to the region covered by the sloshing. In other words, at the scale of the sloshing, heat conduction in the circumferential direction can be neglected.

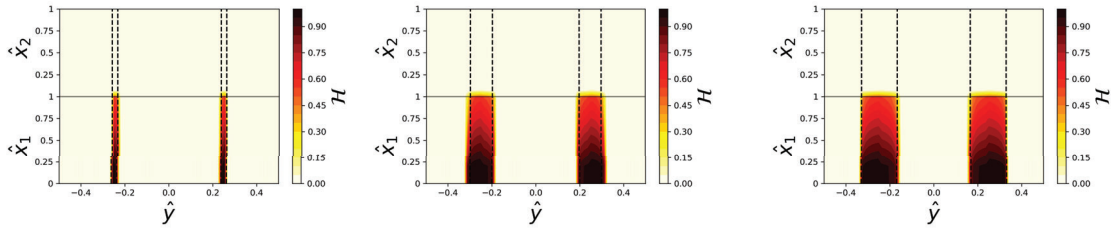

(a) $\hat{A}_f = 0.016$ (b) $\hat{A}_f = 0.064$ (c) $\hat{A}_f = 0.087$

Figure 8: 2D contour plot of transfer function value of a dual-layered cryogenic tank wall subjected to sloshing excitation of different non-dimensional amplitudes.

https://doi.org/10.52202/069564-0032

4. Conclusions

This study analyzed the transient heat conduction with cryogenic sloshing perturbation within a multi-layered tank, considering both one and two-dimensional cases. A dimensionless analysis was performed to identify the scaling parameters on the thermal behavior of the tank.

The study identified a threshold on the Fourier number for inner layer material, namely $Fo_1 \approx 3 \times 10^{-1}$, above which the thermal excitation is amplified and crosses the entire layer thickness. This amplification is attributed to the inner wall overheating due to heat ingress from the outside. It can be minimized by increasing the insulation, i.e. decreasing the Fourier number of the ambient side material Fo_2. This finding suggests that careful consideration must be given to the thermal properties of the tank walls and the operating conditions to minimize the effects of sloshing on the thermal cycling of the inner tank shell.

Furthermore, the study revealed that the perturbation caused by sloshing remains localized in the excitation region and barely spreads along the circumference of the inner shell. This means that the time scale of the sloshing is usually much shorter than the time scale for the heat conduction in the circumferential direction for most material combinations considered in this work.

Overall, the single and multi-layered tank walls' dimensionless analysis has provided an understanding of the thermal behavior of cryogenic storage tanks subjected to sloshing. In particular, thermal modulation and penetration depth maps are valuable tools for designers. The maps can be used to determine the tank's response to such perturbation excitation as a function of the Fourier number of each layer and can help optimize the design of the tank walls by minimizing the effects of sloshing on the temperature distribution within the tank. The findings of this study can be used to improve the design and operation of cryogenic storage systems, to enhance their safety and efficiency. Further research will be focused on extending this work to a complete thermodynamic model accounting for fluid phase and temperature changes.

Acknowledgments

This work has been funded by the Flemish Agentschap Innoveren & Ondernemen in the framework of the cSBO project HBC.2021.0680 "Clean Hydrogen Propulsion for Ships (CHyPS)". Pedro Marques is supported by the FRIA grant 40009348 from the 'Fonds de la Recherche Scientifique (F.R.S. -FNRS)'. The authors gratefully acknowledge the fruitful conversations with Prof. Jean Marie Buchlin on unsteady heat conduction.

Nomenclature

Letter symbols

A	sloshing amplitude, m
$\mathcal{C}$	interface location at rest, m
c_p	specific heat capacity, J/(kgK)
$\hat{d}$	dimensionless penetration depth
f	liquid fill height, m
Fo	Fourier number
g	gravitational acceleration, m/s^2
Gr	Grashof number
h	heat transfer coefficient, W/(m^{2}K)
$\mathcal{H}$	thermal modulation
Nu	Nusselt number
e	tank wall thickness, m
Pr	Prandtl number
R	tank radius, m
Ra	Rayleigh number
Re	Reynolds number
Ri	Richardson number

https://doi.org/10.52202/069564-0032

T temperature, K

U fluid velocity, m/s

Greek symbols

α thermal diffusivity, m^2/s

β volumetric thermal expansion, K^{-1}

ε tank aspect ratio

ρ density, kg/m^3

ν kinematic viscosity, m^2/s

κ thermal conductivity, W/(mK)

θ dimensionless temperature

ω sloshing frequency, rad/s

Subscripts and superscripts

f fluid

g gas

l liquid

i interface

a ambient

References

[1] Heathman JH, Nau RA, Yates GB, Egli WA, Christian JL, Neff D, Rose J, and Stockham TL. *Hydrogen tankage for hypersonic cruise vehicles - Phase 1*. Technical report. General Dynamics San Diego CONVAIR DIR, 1966 Aug

[2] Murugan S, Starvin MS, and Dhas K. *Thermo structural analysis of high pressure cryogenic tank*. International journal of engineering research and technology 2013; 2

[3] Rao KS and Jagadeesh C. *Analysis of Thermal Criteria on Cryogenic Pressure Vessel.* International Journal of Trend in Scientific Research and Development 2019

[4] Ko W. *Thermocryogenic buckling and stress analyses of a partially filled cryogenic tank subjected to cylindrical strip heating.* NASA Technical Memorandum 4579, 1994

[5] Craig S and Hanna G. *Thermal Modeling and Analysis of a Cryogenic Tank Design Exposed to Extreme Heating Profiles.* Technical report NASA Dryden Flight Research Facility, 1991

[6] Mital S, Gyekenyesi J, Arnold S, Sullivan R, Manderscheid J, and Murthy P. *Review of Current State of the Art and Key Design Issues with Potential Solutions for Liquid Hydrogen Cryogenic Storage Tank Structures for Aircraft Applications.* Technical report NASA-TM-2006-214346., 2006

[7] Stroe ME. *Hydrogen embrittlement of ferrous materials.* PhD thesis. Université libre de Bruxelles, Faculté des sciences appliquées – Matériaux, 2005

[8] Pressouyre G. *Trap theory of Hydrogen embrittlement.* Acta Metallurgica 1980; 28:895–911. DOI: 10 . 1016 / 0001 - 6160(80) 90106 - 6.

[9] Winnefeld C, Kadyk T, Bensmann B, Krewer U, and Hanke-Rauschenbach R. *Modelling and Designing Cryogenic Hydrogen Tanks for Future Aircraft Applications.* Energies 2018 Jan; 11:105. DOI: 10.3390/en1101005

[10] Zielinski A. *Hydrogen-assisted degradation of some non-ferrous metals and alloys.* Journal of Materials Processing Technology 2001 Feb; 109:206–14.

[11] Johnson WL, Balasubramaniam R, and Grotenrath R. *Analysis of heat transfer from a local heat source at cryogenic temperatures.* IOP Conference Series: Materials Science and Engineering 2022 May; 1240:012013. DOI: 10.1088/1757- 899X/1240/1/012013.

[12] Lin C and Hasan M. *Self-pressurization of a spherical liquid hydrogen storage tank in a microgravity environment.* 30th Aerospace Sciences Meeting and Exhibit. DOI: 10.2514/6.1992-363. eprint: https://arc.aiaa.org/doi/pdf/10.2514/6.1992-363.

[13] Seo M and Jeong S. *Analysis of self-pressurization phenomenon of cryogenic fluid storage tank with thermal diffusion model.* Cryogenics 2010; 50. 2009 Space Cryogenic Workshop:549–55. DOI: 10.1016/j.cryogenics.2010.02.021.

[14] Kartuzova O, Kassemi M, Umemura Y, Kinefuchi K, and Himeno T. *CFD Modeling of Phase Change and Pressure Drop during Violent Sloshing of Cryogenic Fluid in a Small-Scale Tank.* AIAA Propulsion and Energy Forum, 2020

[15] Mukai Y and Nishinura A. *Mechanical Properties of SUS304 Stainless Steel Under Cold Thermal Cycles.* 11th International Conference on Magnet Technology (MT-11): Volume 1. Ed. by Sekiguchi T and Shimamoto S. Dordrecht: Springer Netherlands, 1990 :743–8. DOI: 10.1007/978- 94- 009- 0769- 0128.

[16] Miles JW. *Resonantly forced surface waves in a circular cylinder.* Journal of Fluid Mechanics 1984; 149:15–31.

[17] Lamb H. *Hydrodynamics. 3rd ed.* Cambridge University Press, 1945

[18] Churchill SW and Chu HH. *Correlating equations for laminar and turbulent free convection from a horizontal cylinder.* International Journal of Heat and Mass Transfer 1975; 18:1049–53. DOI: 10.1016/0017-9310(75)90222- 7

[19] Ludwig C, Dreyer M, and Hopfinger E. *Pressure variations in a cryogenic liquid storage tank subjected to periodic excitations.* International Journal of Heat and Mass Transfer 2013 Aug; 66:223–34.

[20] Bergman TL, Lavine AS.,*Fundamentals of heat and mass transfer*. 7th ed. John Wiley & Sons, 2011

[21] Bell IH, Wronski J, Quoilin S, and Lemort V. *Pure and Pseudo-pure Fluid Thermophysical Property Evaluation and the Open-Source Thermophysical Property Library CoolProp*. Industrial & Engineering Chemistry Research 2014; 53:2498–508. DOI: 10.1021/ie4033999.

[22] Verstraete D. *The Potential of Liquid Hydrogen for long range aircraft propulsion.* PhD thesis. Cranfield University, 2009

[23] Prasad K, Kramer R, Marsh N, Nyden M, Ohlemiller T, and Zammarano M. *Numerical simulation of fire spread on polyurethane foam slabs.* Conference Proceedings - Fire and Materials 2009, 11th International Conference and Exhibition 2009 Jan; 28

[24] Araujo J, Waldman W, and De Paoli M. *Thermal properties of high density polyethylene composites with natural fibres: Coupling agent effect*. Polymer Degradation and Stability 2008; 93:1770–5

[25] Hindmarsh A and Petzold L. *LSODA, Ordinary Differential Equation Solver for Stiff or Non-Stiff System.*, 2005

[26] Virtanen P, Gommers R, Oliphant TE, Haberland M, Reddy T, Cournapeau D, Burovski E, Peterson P, Weckesser W, Bright J, van der Walt SJ, Brett M, Wilson J, Millman KJ, Mayorov N, Nelson ARJ, Jones E, Kern R, Larson E, Carey CJ, Polat I, Feng Y, Moore EW, VanderPlas J, Laxalde D, Perktold J, Cimrman R, Henriksen I, Quintero EA, Harris CR, Archibald AM, Ribeiro AH, Pedregosa F, van Mulbregt P, and SciPy 1.0 Contributors. *Fundamental Algorithms for Scientific Computing in Python.* Nature Methods 2020; 17:261–72.

[27] Meneghelli B, Tamburello D, Fesmire J, and Swanger A. *Integrated Insulation System for Automotive Cryogenic Storage Tanks.* Technical report IV.D.4. Kennedy Space Center, 2016

[28] Swanger A, Notardonato W, and Jumper K. *ASME Section VIII Recertification of a 33,000 Gallon Vacuum-Jacketed LH2 Storage Vessel for Densified Hydrogen Testing at NASA Kennedy Space Center* NASA Kennedy Space Center. 2015

https://doi.org/10.52202/069564-0032